



ARTICLE

Feedback inhibition of actin on Rho mediates content release from large secretory vesicles

Dagan Segal¹ , Assaf Zaritsky^{2,3} , Eyal D. Schejter¹, and Ben-Zion Shilo¹ 

Secretion of adhesive glycoproteins to the lumen of *Drosophila melanogaster* larval salivary glands is performed by contraction of an actomyosin network assembled around large secretory vesicles, after their fusion to the apical membranes. We have identified a cycle of actin coat nucleation and disassembly that is independent of myosin. Recruitment of active Rho1 to the fused vesicle triggers activation of the formin Diaphanous and actin nucleation. This leads to actin-dependent localization of a RhoGAP protein that locally shuts off Rho1, promoting disassembly of the actin coat. When contraction of vesicles is blocked, the strict temporal order of the recruited elements generates repeated oscillations of actin coat formation and disassembly. Interestingly, different blocks to actin coat disassembly arrested vesicle contraction, indicating that actin turnover is an integral part of the actomyosin contraction cycle. The capacity of F-actin to trigger a negative feedback on its own production may be widely used to coordinate a succession of morphogenetic events or maintain homeostasis.

Introduction

Coordinated formation and disassembly of contractile actin-based structures has been shown to underlie diverse settings of tissue morphogenesis. These events are not regulated directly by gene expression, but rather rely on inherent mechanistic features, as well as responses to tension and stress (Guillot and Lecuit, 2013; Pandya et al., 2017). The tight temporal and spatial regulation of actomyosin dynamics mediating such cascades of cellular contractile events, and the versatile activity of the same basic machinery in diverse biological scenarios, remain to be fully understood.

Exocytosis from the epithelium of *Drosophila melanogaster* larval salivary glands provides a powerful system to study the orchestrated regulation of actomyosin during contractile events (Tran and Ten Hagen, 2017). Upon stimulation by hormonal cues, these cells secrete large amounts of “glue” glycoproteins from their apical membrane into the lumen of the gland over the course of 2 h, in preparation for external deposition that will enable the larva to adhere to a dry surface before pupariation (Biyasheva et al., 2001). The glue proteins are stored before secretion in very large vesicles, ranging in size from 4 to 8 μm in diameter. Content release from these vesicles into the lumen is achieved after their fusion with the apical membrane of the cell, through formation of an actin coat around each vesicle and recruitment of myosin, which together mediate the forces

necessary for vesicle contraction (Tran et al., 2015; Rouso et al., 2016; Fig. 1, a and b).

The basic molecular network underlying this actomyosin-dependent secretion process, which lasts ~ 3 min for each vesicle, has been established (Tran et al., 2015; Rouso et al., 2016). Upon fusion with the apical membrane, activated Rho1-GTP is enriched on the fused vesicle and subsequently recruits and activates the formin Diaphanous (Dia), which in turn generates an actin coat around the vesicle. In parallel, Rho1 triggers Rho kinase (ROCK; Rok in *Drosophila*), which recruits myosin onto the actin coat and mediates contraction. Each vesicle releases its content after fusion, and the dense actomyosin network surrounding it disintegrates. Thus, every secretory glue vesicle presents an entire cycle of actomyosin coat assembly and disassembly lasting ~ 4 min, providing a unique system to identify the relevant molecular players and to dissect their regulatory interactions.

We have found that disassembly of the actin coat, which accompanies vesicle content release, is necessary for contraction of the actomyosin network. A dedicated Rho GTPase activating protein (RhoGAP) mediates Rho1 inactivation, leading to actin disassembly. RhoGAP activity and recruitment to the contracting vesicle appear to depend on F-actin, implying a negative feedback-based mechanism. The sequential temporal recruitment of active Rho1 and its inhibitors is made evident by the multiple

¹Department of Molecular Genetics, Weizmann Institute of Science, Rehovot, Israel; ²Department of Molecular Cell Biology, Weizmann Institute of Science, Rehovot, Israel; ³Lyda Hill Department of Bioinformatics, University of Texas Southwestern Medical Center, Dallas, TX.

Correspondence to Ben-Zion Shilo: benny.shilo@weizmann.ac.il.

© 2018 Segal et al. This article is distributed under the terms of an Attribution–Noncommercial–Share Alike–No Mirror Sites license for the first six months after the publication date (see <http://www.rupress.org/terms/>). After six months it is available under a Creative Commons License (Attribution–Noncommercial–Share Alike 4.0 International license, as described at <https://creativecommons.org/licenses/by-nc-sa/4.0/>).

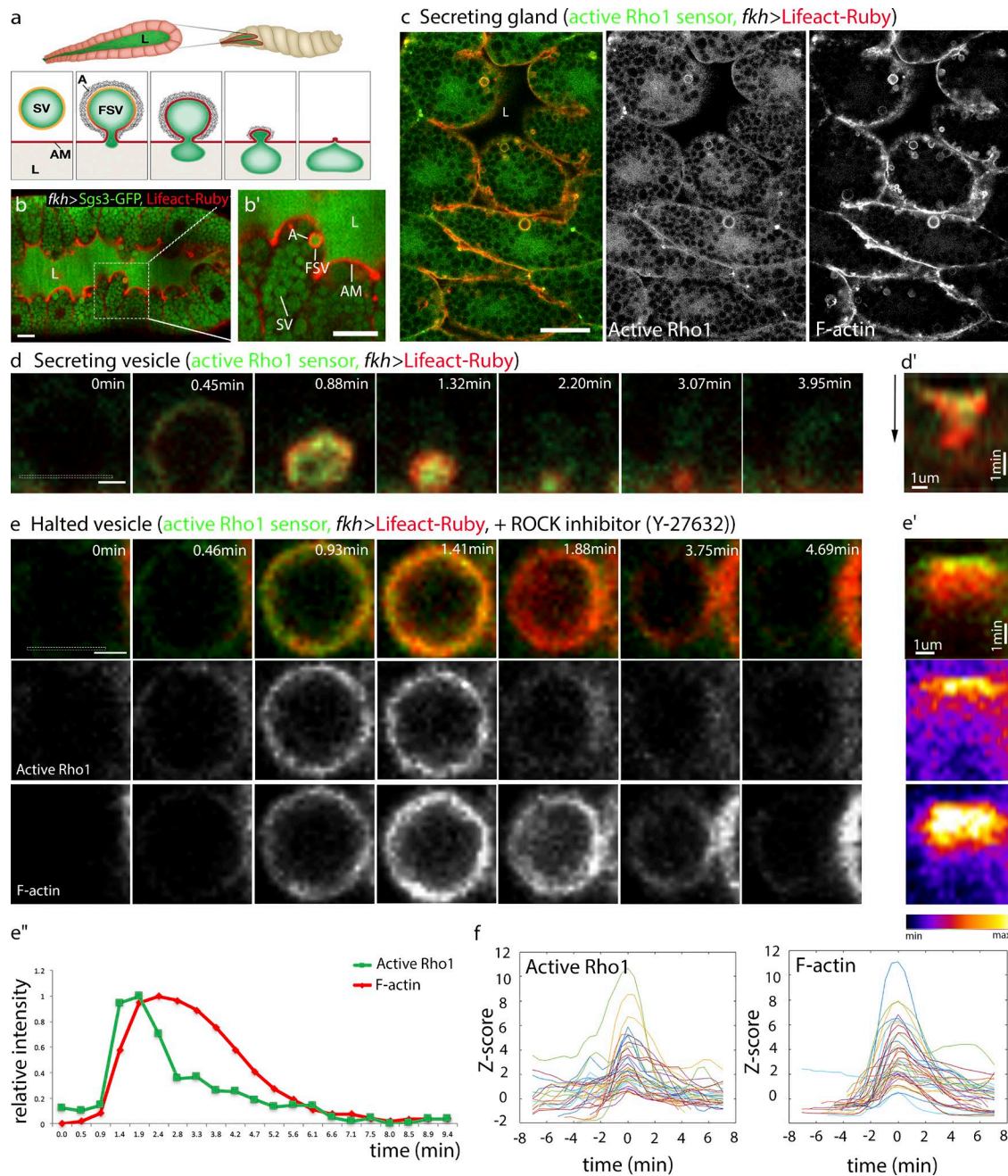


Figure 1. Actin recruitment and disassembly are driven by the activity of Rho1. (a–b') Schematic drawing (a) and confocal microscope image (b) of a *Drosophila* third-instar salivary gland expressing the glue protein Sgs3-GFP (green) and the F-actin marker LifeAct-Ruby (red; A). (b') Enlargement of boxed area in b. Large secretory cells surround an expanding lumen (L) and are filled with secretory vesicles (SV) containing the glue cargo. During secretion, vesicles fuse to the actin-rich apical membrane (AM) facing the lumen. Fused secretory vesicles (FSV) form an actomyosin coat (A) that enables contraction and expulsion of their content into the lumen. (c) A secreting gland displays active Rho1 (visualized by the sensor Ani-RBD-GFP [Munjál et al., 2015], green) and F-actin (red) enriched on vesicles that fused to the apical membrane, at various stages of contraction. (d) Time course of a single secreting vesicle. The vesicle contracts fully within 3 min, with residual actin cleared from the site of fusion after ~1 additional minute. (d') Kymograph monitoring active Rho1 and F-actin dynamics at the vesicle/plasma membrane interface (dashed-box area in initial panel of d). Time progresses downward as indicated by black arrow. Dynamics of actin clearing are difficult to characterize because of drastic morphological changes. (e) Addition of the ROCK inhibitor Y-27632 causes accumulation of contraction-halted vesicles, allowing unperturbed visualization of active Rho1 and actin dynamics (see also Video 1). Halted vesicles exhibit active Rho1 and actin coat enrichment, followed by Rho1 inactivation and actin coat disassembly, in a time frame comparable to that of a squeezing vesicle. (e') Kymographs monitoring active Rho1 and F-actin dynamics at the vesicle surface (dashed-box area in initial panel of e). (e'') Graph plotting relative intensity of active Rho1 (green) and F-actin (red) in the area monitored in the kymographs (e') over time. Intensity is normalized to the highest value within each channel. Note that both active Rho1 and actin rise sharply, but actin disassembly is gradual whereas Rho1 inactivation is sharp. (f) Dynamic profiles over time of active Rho1 and F-actin in 38 vesicles from a single contraction-halted gland. Vesicle time scales are aligned to intensity peaks. Z-score is defined as the number of standard deviations that the signal intensity differs from background levels. The duration and dynamics of active Rho1 and actin are highly similar between vesicles, despite large variations in z-score. Bars: (b, b', and c) 20 μ m; (d and e) 2 μ m.

cycles of accumulation and dispersion of active Rho1 and the actin coat observed on individual fused but contraction-halted vesicles. Actin coat dynamics and the resulting vesicle contraction are therefore achieved by coordinating formation and disassembly of the actomyosin network.

Results

Actin recruitment and disassembly is driven by the activity of Rho1

We examined the dynamics of actin recruitment and its regulators on secretory vesicles through live, ex vivo imaging of the *Drosophila* salivary gland. Previously, we have shown that stimulation of Dia nucleation activity by active Rho1 is required for generation of the bulk of the actin coat surrounding the secretory vesicles (Rousso et al., 2016). Myosin II is also recruited to the vesicle in a Rho1/Rok-dependent manner (Rousso et al., 2016), thereby forming the actomyosin network necessary for vesicle contraction. Concomitant with squeezing of the vesicle, actin as well as active Rho1 are cleared from the vesicle surface (Fig. 1, c and d).

The rapid reduction in size of the vesicle as it contracts, and the enriched levels of filamentous actin continuously present on the apical membrane, make it difficult to reproducibly follow the dynamics of actin disassembly on the vesicle. We therefore used a chemical inhibitor of ROCK kinase activity (Y-27632; Uehata et al., 1997) to hinder myosin II activation, with the aim of preventing vesicle contraction and uncoupling it from actin coat disassembly, thereby enabling clearer visualization and quantification of actin dynamics on the vesicles that fail to squeeze. Glands treated with Y-27632 or other drugs (see Materials and methods) were imaged from the onset of drug addition to facilitate analysis without allowing accumulation of adverse effects.

After treatment with Y-27632, vesicles still fuse with the apical membrane, and an actin coat is formed around them (Fig. 1 e). However, myosin II is not recruited, and 60% of vesicles fail to contract (Fig. S1 and Video 1). The contraction-halted vesicles display a cycle of actin assembly and disassembly, which, importantly, exhibits a time course that is comparable to that of a squeezing vesicle (Fig. 1 d). Similar effects have been observed upon knockdown of *rok* by RNAi (Rousso et al., 2016). Notably, actin disassembly is also observed upon knockdown of the *Drosophila* myosin II (heavy chain) homologue *zipper* (Rousso et al., 2016). This implies that the effects of Rok inhibition by Y-27632 result from blocking actomyosin-mediated vesicle constriction, rather than regulation of actin turnover (e.g., by affecting the activity of the actin-severing protein Cofilin; Maekawa et al., 1999). These features make the halted vesicles a useful setting for studying actin coat dynamics and, furthermore, demonstrate that actin disassembly is independent of myosin II or vesicle contraction.

Monitoring of the An1-RBD-GFP sensor revealed that active Rho1 levels associated with the halted vesicles not only rise but also diminish, and do so in concert with the dynamics of actin coat assembly and disassembly (Fig. 1 e). Semiautomated quantification on multiple vesicles within a single gland (Fig. 1 f) or multiple glands (Fig. S2; see Materials and methods) allowed

further characterization of these active Rho1 and actin cycles. Cycle duration commonly ranged from 1 to 3 min for active Rho1 and 3 to 7 min for actin (Fig. S2 a), despite large variations in signal amplitude (Fig. 1 f). This is comparable to the time scale of content release by a naturally contracting vesicle, which takes place over 1–3 min, with subsequent actin clearing taking roughly one additional minute (Rousso et al., 2016; Fig. 1 d). More detailed analysis showed that Rho1 inactivation precedes actin coat disassembly (Fig. S2 b). These quantifications suggest that the assembly and disassembly of the actin cycle are dependent on Rho1 activity: actin coat assembly is triggered (via Dia) after Rho1 activation (Rousso et al., 2016), whereas coat depletion follows shutdown of Rho1 activation and a resulting shift toward filament depolymerization.

RhoGAP71E is required for Rho1 inactivation

Because Rho1 inactivation precedes and likely leads to actin coat disassembly, we examined the potential involvement of RhoGAPs, which commonly facilitate the conversion of RhoGTPases from an active GTP-bound to an inactive GDP-bound state (Tcherkezian and Lamarche-Vane, 2007). Although *Drosophila* has more than 20 RhoGAP proteins (Greenberg and Hatini, 2011), RNA sequencing data suggest that only a subset of eight RhoGAPs are expressed in the salivary gland at high or moderate levels (Brown et al., 2014). We conducted a functional knockdown screen, by monitoring active Rho1 sensor and actin coat dynamics on contraction-halted vesicles, after salivary-gland expression of RNAi constructs directed against each of the eight RhoGAP genes (Table S1).

A unique pattern of sustained Rho1 activation and a persistent actin coat, the predicted phenotype for interference with Rho1 inactivation, was observed after knockdown of only one of these elements, RhoGAP71E (also termed C-GAP; Mason et al., 2016). Vesicles in Y-27632-treated salivary glands expressing *RhoGAP71E* RNAi displayed sustained presence of active Rho1 sensor and actin coat for several minutes (Fig. 2, a and b). Three different RNAi constructs targeted against RhoGAP71E showed similar results (Table S1). Despite variable penetrance of *RhoGAP71E* knockdown in different larvae, quantifications of many contraction-halted vesicles showed significantly longer sustainment of the actin coat compared with control (Figs. 2 b and S2 c). In contrast, the active Rho1/actin cycles on contraction-halted vesicles were not affected by expression of all other RhoGAP RNAi constructs (for example, Fig. S3 a). The variable penetrance of *RhoGAP71E* knockdown is consistent with a partial silencing effect of the RNAi and possible contributions of some of the other RhoGAP proteins.

RhoGAP71E has been implicated in spatial restriction of Rho1 activity and subsequent cell contraction during gastrulation of *Drosophila* embryos (Mason et al., 2016). To follow the role of RhoGAP71E in regulation of Rho1 activity in glue vesicles, we sought to examine its dynamic localization on the secretory vesicles. Toward this end, we used the recombinase-mediated cassette exchange technique (Venken et al., 2011) to insert GFP into the *RhoGAP71E* gene locus, thereby generating an endogenously expressed, GFP-tagged version. The tagged version is functional, as indicated by viability of homozygous flies.

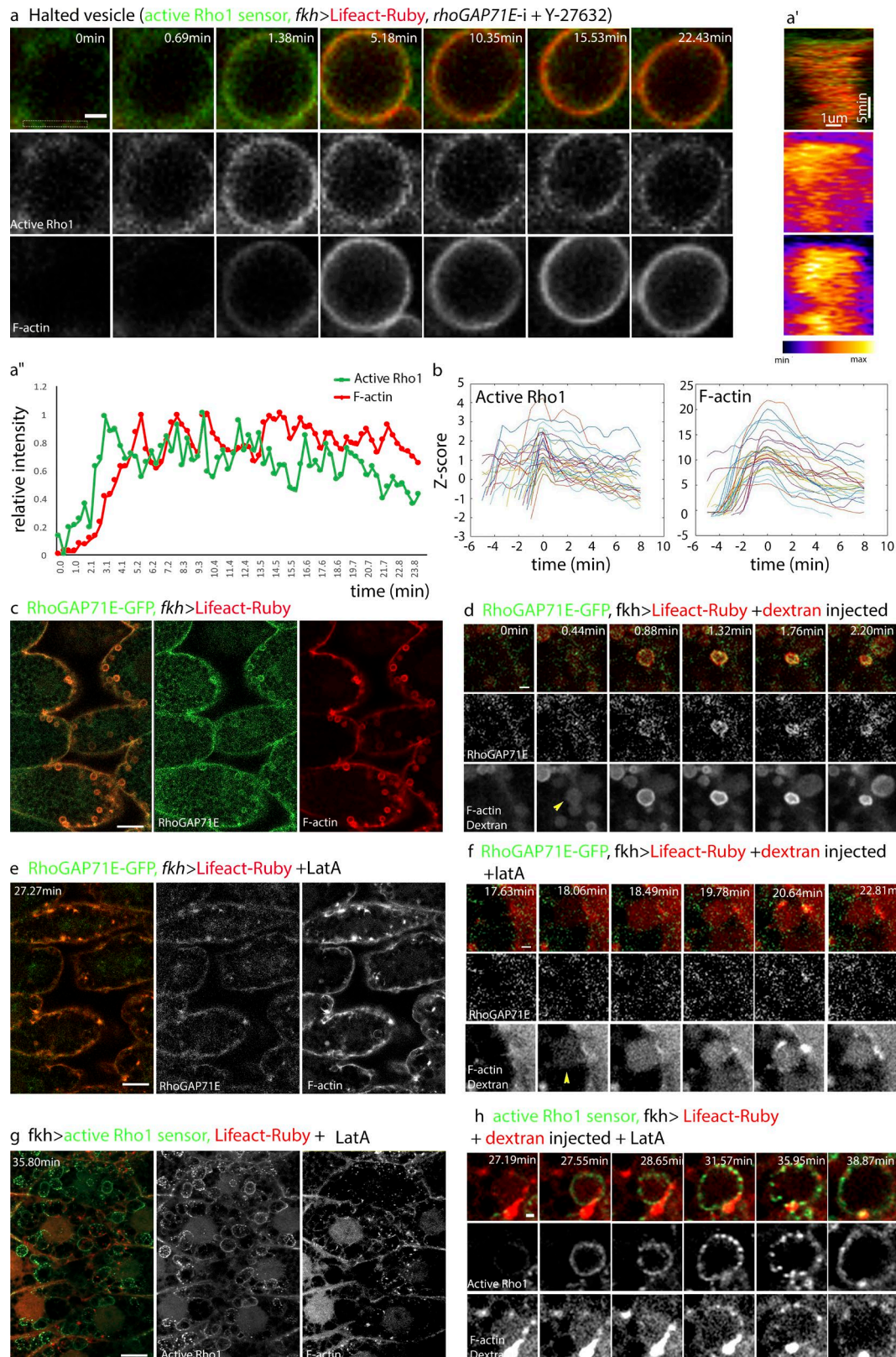


Figure 2. RhoGAP71E is required for Rho1 inactivation. A candidate-based RNAi screen identified RhoGAP71E as a regulator of Rho1 inactivation in the salivary gland. **(a)** Contraction-halted glands expressing the sensor for active Rho1 (green) and LifeAct-Ruby (red) along with *RhoGAP71E* RNAi (VDRCL09797) show sustained active Rho1 and actin coat. **(a')** Kymographs monitoring active Rho1 and F-actin dynamics at the vesicle surface (dashed-box area in initial panel of a). **(a'')** Graph plotting relative intensity of active Rho1 (green) and F-actin (red) in the area monitored in the kymographs (a') over time. Intensity is normalized to the highest value within each channel. Note that both active Rho1 and actin rise sharply and are sustained on the vesicle for >20 min. **(b)** Dynamic profiles

RhoGAP71E-GFP is recruited to most fused vesicles displaying an actin coat (Fig. 2 c). We monitored the onset of vesicle fusion with the apical membrane by injection of fluorescent dextran into the salivary gland lumen, because the dye enters the vesicle immediately upon fusion (Rousso et al., 2016). Using this method, we followed the temporal dynamics of RhoGAP71E-GFP during secretion, which appears to be recruited to the vesicles after fusion and concurrently with assembly of the actin coat (Fig. 2 d). Subsequent higher-time-resolution imaging showed that RhoGAP71E is, on average, recruited slightly after the onset of actin coat formation, with a median time delay of 4.8 ± 10.2 s (Fig. S3 c). Contraction-halted vesicles (Y-27632 treated) from glands homozygous for *RhoGAP71E-GFP* still display actin disassembly, indicating that the tagged protein is functional in this context. Notably, RhoGAP71E is removed once the actin coat is disassembled (Fig. S3 b).

Recent work in the early *Caenorhabditis elegans* embryo has suggested that actin can serve as a recruiting element for RhoGAPs (Robin et al., 2016 Preprint). To determine whether actin plays a similar role in the context of glue vesicle secretion, we examined the effects of inhibition of actin polymerization, using the chemical inhibitor latrunculin A (LatA). Actin-coated vesicles are no longer observed after 20 min of LatA addition (Fig. 2 e). Dextran injection to the lumen of such LatA-treated glands demonstrates that vesicle fusion is unaffected (Fig. 2 f), although, as expected, these vesicles do not contract, because they lack an actomyosin coat. LatA treatment does not, however, prevent recruitment of active Rho1, which is present on many of these vesicles, albeit with a somewhat irregular spatial pattern (Fig. 2, g and h; and Video 2). Monitoring the effects of LatA treatment on multiple vesicles reveals that the active Rho1 sensor is found to persist on ~39% of fused vesicles (Fig. S3 d). This suggests that enrichment of active Rho1 is independent of actin coat formation, consistent with its role in triggering actin polymerization. In contrast, RhoGAP71E-GFP recruitment was abolished entirely in newly fused vesicles lacking an actin coat (Fig. 2, e and f). Collectively, these results suggest that although Rho1 activation is independent of F-actin, RhoGAP71E recruitment and subsequent Rho1 inactivation are F-actin dependent.

Coordinated oscillations of active Rho1, actin, and RhoGAP71E

Strikingly, prolonged tracking of individual contraction-halted vesicles uncovered coordinated oscillations of active Rho1 and F-actin upon a large subset of halted vesicles (Fig. 3, a–a’), a phenomenon previously observed after expression of *rok* or *zipper* RNAi constructs (Rousso et al., 2016). Because these vesicles continue to be fused to the apical membrane, which provides a permanent source of active Rho1 (Rousso et al., 2013), the observed additional cycles of actin coating on the same vesicle may be a consequence of initial disassembly of the actin coat and the concomitant loss of RhoGAP71E (Fig. 2). Automated scoring of vesicles for oscillations (see Supplemental Methods) showed that 52.9% of vesicles that were tracked for ≥ 15.5 min displayed at least one oscillation in addition to the initial complete actin cycle, with several cases of two or more oscillations on the same vesicle (for example, Fig. S4 a). The median time interval between oscillations was ~6 min (Fig. 3 b), which is similar in time scale to a single actin cycle (Fig. S2). Notably, instances of oscillations of actin can also be observed on contracting vesicles, although these events require an increased temporal resolution and are challenging to resolve from the cortical actin associated with the apical membrane (Fig. S4 b).

Importantly, RhoGAP71E-GFP recruitment to contraction-halted vesicles also exhibits an oscillatory behavior, in apparent coordination with the repeated actin cycles (Fig. 3 c). Collectively, these results suggest that Rho1, the actin coat, and RhoGAP71E are all part of a shared regulatory circuitry, and are sequentially recruited. This temporally resolved regulatory cycle appears to be initiated by Rho1 activation, which subsequently recruits actin and RhoGAP71E to the vesicle, and ultimately leads to Rho1 inactivation and actin disassembly with a temporal delay comparable to the time of a squeezing vesicle. In constricting vesicles, such a cycle typically operates only once.

Actin disassembly is essential for vesicle contraction

We next sought to assess the role of the Rho1-actin-RhoGAP71E regulatory network, which we had identified on contraction-halted vesicles, in the context of normal glue content release. Although formation of the Rho1-dependent actomyosin

over time of active Rho1 and F-actin in 29 vesicles from a single contraction-halted gland. Vesicle time scales are aligned to intensity peaks. Z-score is defined as the number of standard deviations that the signal intensity differs from background levels. Note that although Rho1 and actin rise sharply, they are sustained above initial levels over many minutes (compare time scale to Fig. 1 f). (c) Glands expressing RhoGAP71E-GFP, an endogenously expressed GFP-tagged version of RhoGAP71E (green) and LifeAct-Ruby (red). RhoGAP71E-GFP appears to be enriched in most actin-coated vesicles. (d) A single secreting vesicle in such a gland expressing RhoGAP71E-GFP (green) and LifeAct-Ruby (red), with TMR-dextran (red) injected into the lumen to mark fused vesicles. Yellow arrowhead marks appearance of dextran within the vesicle, preceding formation of the bright actin coat on the vesicle surface. RhoGAP71E-GFP and actin appear to be simultaneously enriched on vesicles within 30 s after vesicle fusion. (e) Glands expressing RhoGAP71E-GFP (green) and LifeAct-Ruby (red). Addition of the F-actin polymerization inhibitor LatA to the medium caused loss of both actin coat formation and RhoGAP71E recruitment to vesicles. Time corresponds to time elapsed since LatA addition. (f) A single secreting vesicle in such a LatA-treated gland expressing RhoGAP71E-GFP (green) and LifeAct-Ruby (red), injected with TMR-dextran (red) into the lumen. Yellow arrowhead marks appearance of dextran and onset of fusion. Although vesicles still fuse 17 min after LatA addition, actin and RhoGAP71E-GFP are not recruited to newly fused vesicles, demonstrating that RhoGAP71E recruitment requires F-actin. (g) LatA-treated glands expressing the active Rho1 sensor (green) and LifeAct-Ruby (red). Unlike RhoGAP71E-GFP, active Rho1 is enriched on a large subset of vesicles, despite the failed recruitment of actin. (h) A single secreting vesicle in such a LatA-treated gland expressing active Rho1 (green) and LifeAct-Ruby (red), and injected with TMR-dextran (red) into the lumen. Active Rho1 is recruited and sustained on the fused vesicle, with a progressively punctate pattern forming over time. In addition, compound vesicle fusion leads to formation of abnormally large vesicles. Under these conditions, active Rho1 is sustained for at least 8 min in ~39% of vesicles ($n = 85$ in four glands; see also Fig. S3), implying lack of Rho1 inactivation in the absence of actin and RhoGAP71E. Bars: (a, d, f, and h) 2 μ m; (c, e, and g) 20 μ m.

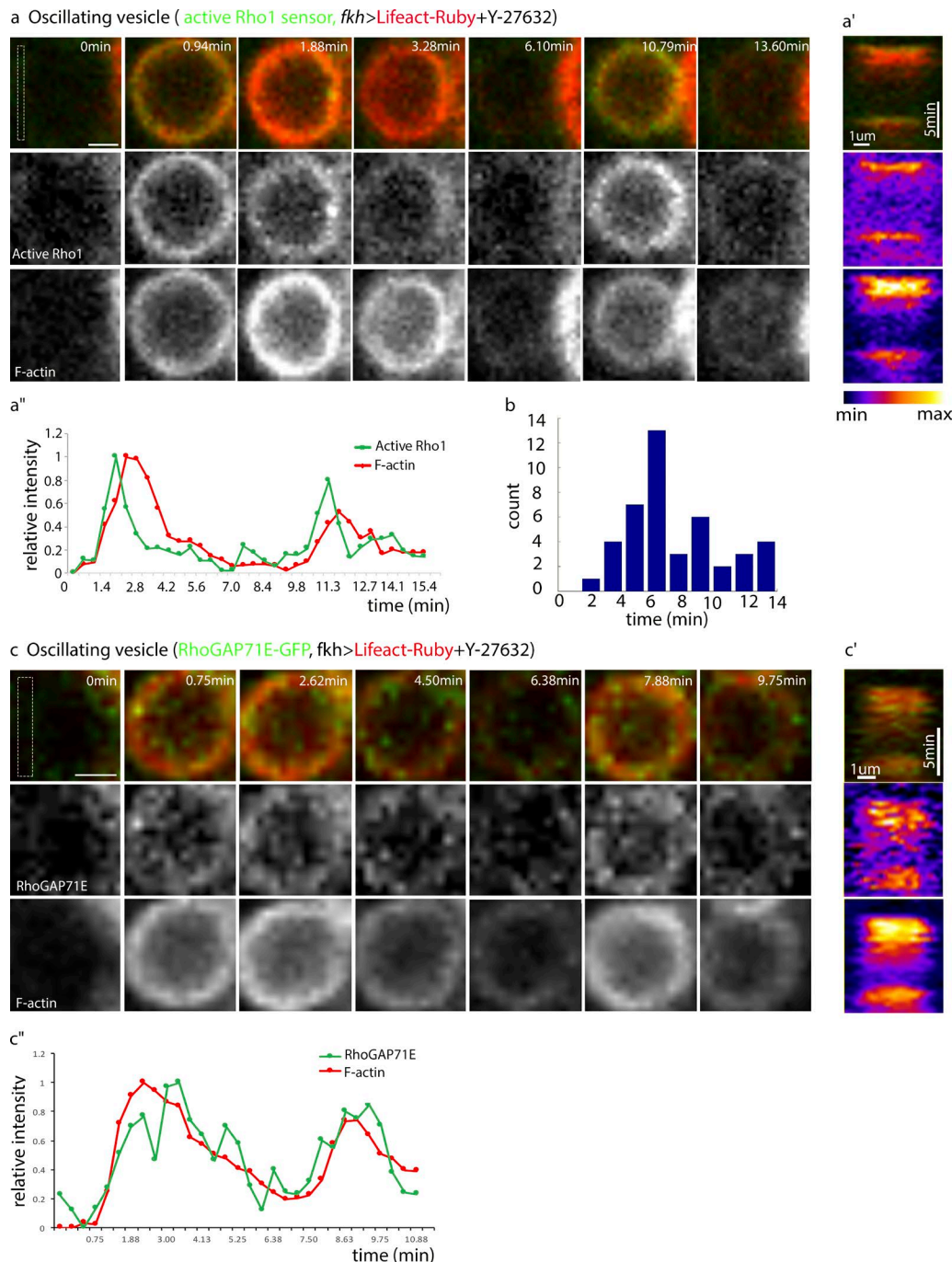


Figure 3. Coordinated oscillations of active Rho1, F-actin, and RhoGAP71E. **(a)** Coordinated oscillatory behavior of the active Rho1 sensor (green) and LifeAct-Ruby (red) on a single contraction-halted vesicle from a Y-27632-treated salivary gland. **(a')** Kymograph monitoring active Rho1 and F-actin dynamics at the vesicle surface (dashed-box area in initial panel of a). **(a'')** Graph plotting relative intensity of active Rho1 (green) and F-actin (red) in the area monitored in the kymograph (a') over time. Intensity is normalized to the highest value within each channel. **(b)** Histogram showing the time in minutes between peaks of actin accumulation in oscillating vesicles ($n = 43$ in four glands). Oscillations most frequently reach their maximum ~ 6 min after the previous peak, similar to the time scale of a single actin cycle. Of vesicles that were tracked for at least 15.5 min (defined by 90th percentile of oscillation peaks + 3 s), 52.9% displayed at least one oscillation in addition to their first peak ($n = 34$ in four glands). **(c)** Coordinated oscillatory behavior of RhoGAP71E-GFP (green) and LifeAct-Ruby (red) on a single contraction-halted vesicle from a Y-27632-treated salivary gland. Coordinated dynamics of actin and RhoGAP71E was observed in 78% of oscillating vesicles ($n = 18$ in three glands). **(c')** Kymograph monitoring RhoGAP71E-GFP and F-actin dynamics at the vesicle surface (dashed-box area in initial panel of c). **(c'')** Graph plotting relative intensity of RhoGAP71E-GFP (green) and F-actin (red) in the area monitored in the kymograph (c') over time. Intensity is normalized to the highest value within each channel. Note that RhoGAP71E-GFP and actin appear and disappear in a similar temporal pattern, consistent with a role for F-actin in RhoGAP71E recruitment. Bars, 2 μm .

coat is essential for vesicle contraction, the significance of coat disassembly is not immediately apparent. We first addressed this issue via knockdown of *RhoGAP71E*, which provides a specific means for sustaining Rho1 activity. Strikingly, this treatment resulted—on its own, without direct inhibition of Rok—in an arrest of secretory vesicle contraction, as seen by accumulation of halted vesicles in the entire gland (Fig. 4 a and Video 3), and failed vesicle constriction in more than 80% of vesicles monitored over time (Figs. 4 b and S5 c). Both active Rho1 and the actin coat persisted on these vesicles, similar to the effect of *RhoGAP71E* knockdown on contraction-halted (Y-27632-treated) vesicles (Fig. 2). In accordance with retention of Rok activity, myosin II was still recruited to the vesicles (Fig. S5, a and b). These observations suggest that Rho1 inactivation is essential for proper actomyosin contraction.

To examine directly the role of actin disassembly in vesicle contraction, we inhibited actin turnover by treatment with the microfilament-stabilizing drug jasplakinolide (Bubb et al., 1994). Contraction-halted vesicles with a persistent actin coat were observed shortly after treatment, again demonstrating the importance of local actin turnover for actomyosin contraction (Fig. 4, c and d; and Fig. S5 c). Active Rho1 was not sustained on these vesicles, suggesting that additional inputs besides persistence of the actin coat contribute to inactivation of Rho1. Notably, prolonged exposure to jasplakinolide gave rise to a second class of halted vesicles, lacking an actin coat, likely caused by depletion of the pool of free actin monomers in the absence of actin turnover (Fig. 4 c and Video 4). These vesicles displayed sustained active Rho1, similarly to what was observed upon addition of LatA and consistent with a role for F-actin in Rho1 inactivation (Fig. 2, g and h).

To further examine the role of actin turnover in vesicle constriction, we interfered with actin polymerization dynamics by manipulating the levels of Chickadee (Chic), the *Drosophila* Profilin homologue (Cooley et al., 1992). Profilin is a key actin monomer-binding protein that affects actin polymerization in a variety of ways, in different cellular contexts (Shields et al., 2014; Rotty et al., 2015; Suarez et al., 2015). Knockdown of *chic* led to formation of abnormally thin, punctate actin coats and an arrest of vesicle contraction (Fig. 4, e–e”; and Video 5), consistent with a role for Profilin-bound actin in mediating the Dia-dependent polymerization underlying coat assembly. Interestingly, overexpression of Chic, presumably increasing Dia-dependent polymerization, also caused defective squeezing (Fig. 4 f and Video 6). These observations suggest that tight regulation of actin polymerization is necessary for proper actomyosin contraction.

Discussion

Exocytosis of adhesive glycoproteins into the lumen of *Drosophila* larval salivary glands serves as an established model for the mechanistic basis of vesicle secretion in tubular organs (Tran and Ten Hagen, 2017). Once the large, cargo-filled secretory vesicles fuse with the apical membrane of the gland epithelial cells, the coordinated recruitment of the actin nucleation machinery and myosin II is essential for vesicle contraction and subsequent content expulsion into the gland lumen (Tran et al., 2015; Rousso et al.,

2016). In this work, we followed the dynamics of actin coating of individual salivary gland secretory vesicles and identified a cycle of Rho1-dependent actin coat assembly and disassembly that is independent of myosin and vesicle constriction. We determined that the time course of a single actin coat assembly/disassembly cycle is roughly similar to that of a contracting vesicle, allowing it to operate within the normal time frame of vesicle contraction. The molecular events underlying the actin cycle are set in motion upon fusion of the vesicle to the apical membrane and recruitment of activated Rho1 to the vesicle surface, triggering both the actin-polymerizing activity of the formin Dia and the recruitment of myosin II (Rousso et al., 2016). The assembled F-actin coat on the fused vesicle then recruits RhoGAP71E, leading to the inactivation of Rho1, resulting in actin coat disassembly. Fig. 5 summarizes the actomyosin cycle that takes place on the fused vesicle.

Importantly, we found that disassembly of the actin coat is a critical aspect of the secretory process, implying that local actin turnover is essential for actomyosin-mediated vesicle contraction. Thus, upon *RhoGAP71E* knockdown, persistent Rho1 activity caused stabilization of the actin coat, leading to failure of vesicle constriction. Similarly, chemical stabilization of the actin coat or enhancement of actin polymerization by overexpression of Profilin also abolished the capacity of the vesicles to squeeze. Actin turnover has been shown to be essential for actomyosin contraction in diverse cellular processes, including cytokinesis in *C. elegans* and fission yeast (Vavylonis et al., 2008; Carvalho et al., 2009), and adjustable adhesion between epithelial cells in *Drosophila* (Jodoin et al., 2015). The requirement for actin disassembly in constriction of secretory vesicles described in this work emphasizes the importance of regulation of actin dynamics across diverse systems.

Why is actin turnover essential for glue vesicle constriction? The actomyosin network in this system faces a significant challenge, in that it must contract and squeeze a large vesicle with a viscous content within a short time frame. We can envision two ways in which actin turnover may play a significant role in facilitating this process. First, actin turnover may be important for dynamic reorganization of myosin as a vesicle contracts. Recent theoretical work has suggested that actin turnover may be important to randomize actomyosin arrays, to avoid stabilization of configurations that are inefficient for contraction (Rubinstein and Mogilner, 2017). For each myosin motor, movement along a single linear actin track may be insufficient for contraction of a large surface area such as that of the vesicle. Dissociation of the actin network may thus allow a motor that has already moved along a given actin track to reorganize along a new track and carry out a new cycle of movement.

Another possible explanation relates to the dynamics of actin nucleation that dictate the balance between linear and branched actin polymerization, because both are essential for vesicle contraction (Tran et al., 2015; Rousso et al., 2016). Under circumstances where monomeric actin (G-actin) is a limiting resource, actin bound by Profilin favors formin-based linear actin over Arp2/3-mediated branched actin assembly (Burke et al., 2014; Suarez et al., 2015). The availability of free G-actin monomers near the fused vesicles may be limiting in this system, as demonstrated by the inability of newly fused vesicles to form an actin coat, once

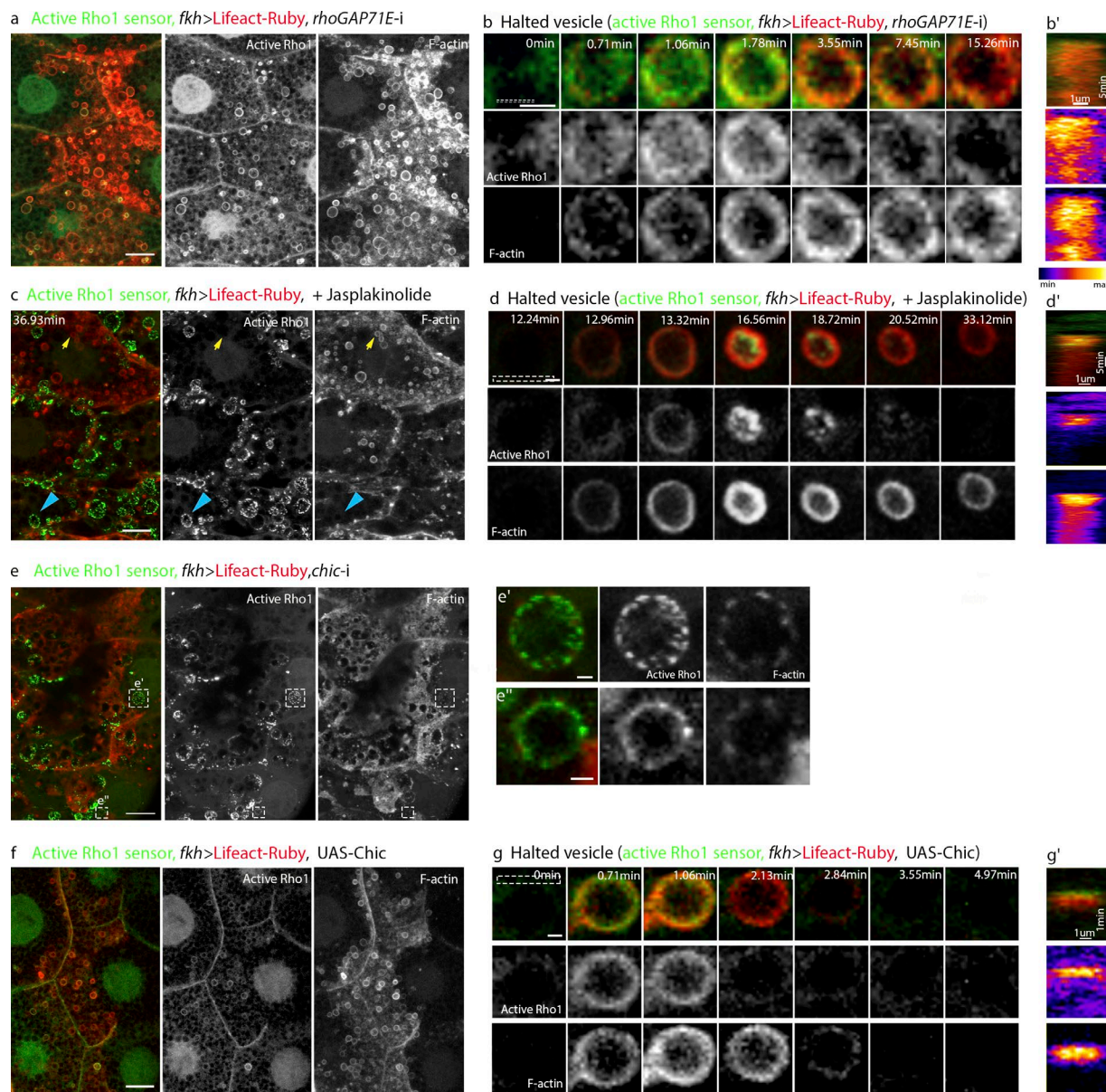


Figure 4. Actin disassembly is essential for vesicle contraction. (a) Salivary glands expressing the active Rho1 sensor (green) and LifeAct-Ruby (red) along with *RhoGAP71E-i* display accumulation of halted vesicles and sustained active Rho1 and F-actin, suggesting that *RhoGAP71E*-dependent Rho1 inactivation is necessary for actin coat disassembly and proper vesicle contraction (see also Video 3). (b) Time course of sustained active Rho1 sensor (green) and LifeAct-Ruby (red) on a single halted vesicle from such a gland. (b') Kymograph monitoring active Rho1 and F-actin dynamics at the vesicle surface (dashed-box area in initial panel of b). (c) Glands expressing the active Rho1 sensor (green) and LifeAct-Ruby (red), treated with the actin-stabilizing drug jasplakinolide. Two types of contraction-halted vesicles can be observed in these glands. Initial fusion events generate halted vesicles that display a sustained actin coat but lose active Rho1 (yellow arrows; see also panel d). Vesicles that fuse after prolonged exposure to the drug display sustained active Rho1 but fail to form an actin coat (blue arrows; see also Video 4). (d) Time course of transient active Rho1 sensor (green) and sustained LifeAct-Ruby (red) on a single halted vesicle from the initial pool generated after drug treatment. Times indicated in panels c and d correspond to time elapsed since drug addition. (d') Kymograph monitoring active Rho1 and F-actin dynamics at the vesicle surface (dashed-box area in initial panel of d). (e–e'') Salivary glands expressing the active Rho1 sensor (green) and LifeAct-Ruby (red) along with *chic-i* display fused contraction-halted vesicles that exhibit enriched active Rho1 but only a weak, punctate actin coat, suggesting that robust actin coat polymerization depends on Chic (see also Video 5). e' and e'' show enlargements of boxed areas in panel e. (f) UAS-driven overexpression of Chic in glands expressing the active Rho1 sensor (green) and LifeAct-Ruby (red) leads to accumulation of contraction-halted vesicles (see also Video 6). (g) Normal time course of the active Rho1 sensor (green) and LifeAct-Ruby (red) on a single halted vesicle from such a gland. (g') Kymograph monitoring active Rho1 and F-actin dynamics at the vesicle surface (dashed-box area in initial panel of g). Bars: (a, c, e, and f) 20 μ m; (b, d, e', and g) 2 μ m.

F-actin was chemically stabilized (Fig. 4). Indeed, overexpression of Profilin, which may shift the balance of actin nucleation toward Dia, blocked vesicle constriction (Fig. 4). Thus, after fusion, the nucleation of actin may be performed primarily by Dia. Once Rho1

activation is blocked by *RhoGAP71E*, the available actin monomers can be channeled to the branched actin nucleation machinery. This model suggests a self-regulatory cascade, where the recruitment of *RhoGAP71E* leads to activation of the branched actin-nucleation

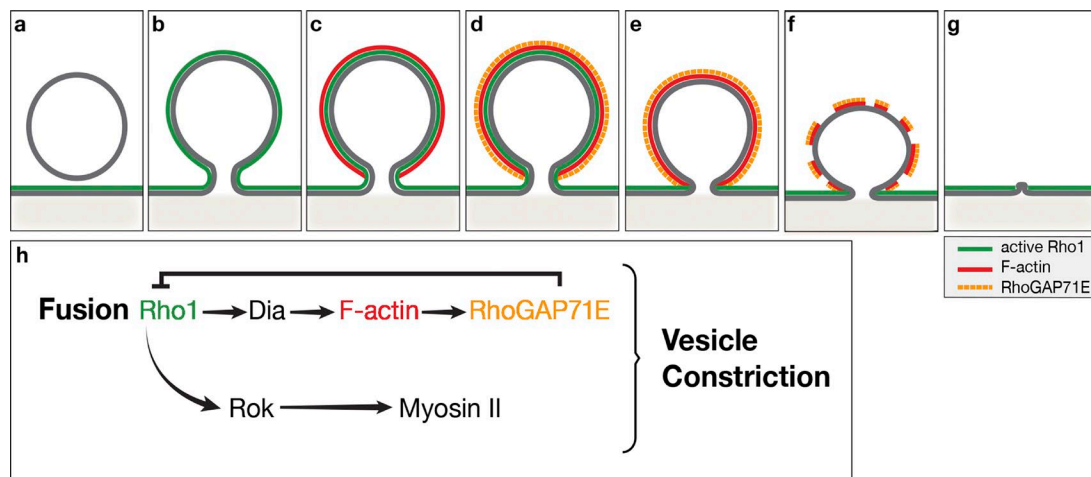


Figure 5. Coordinated formation and disassembly of a contractile actomyosin network mediates content release from large secretory vesicles. A cycle of actin assembly and subsequent depolymerization occurs on a contracting secretory vesicle. The composition of the secretory vesicle membrane is different from the apical salivary gland membrane (a). After vesicle fusion to the apical membrane, active Rho1 is enriched on the vesicle surface (b). Active Rho1 then triggers assembly of the actin coat via Dia (c), which in turn recruits RhoGAP71E (d). RhoGAP71E inactivates Rho1 (e), resulting in actin disassembly (f) and allowing for actomyosin-mediated vesicle constriction (g). Fusion of the vesicle recruits activated Rho1 from the apical membrane (h), leading in parallel to the actin nucleation and depolymerization cycle, to the recruitment of Rok, which triggers myosin II activation. Although Rho1 regulates the recruitment of myosin II to the vesicle, the dynamics of the actin coat are myosin independent. Activities of both arms are essential for vesicle constriction.

machinery. Although the specific role of actin turnover in this system remains an open question, this work demonstrates the need for local actin turnover for proper actomyosin function and suggests a mechanism for its self-organized regulation.

After the onset of actin accumulation on the fused vesicle, the rapid recruitment of RhoGAP71E triggers a negative-feedback circuit to shut down Rho1 activity. This feature raises the necessity to ensure a productive burst of actin nucleation, before Rho1 is inactivated. It will be interesting to determine whether a positive feedback loop is operating in this context, for example, through recruitment of specific activating RhoGEF proteins, similar to their role in stabilizing actin nucleation at the site of bud emergence in *Saccharomyces cerevisiae* (Bidlingmaier and Snyder, 2004; Slaughter et al., 2009).

The feedback cycle of actin assembly and disassembly on the secretory vesicles, mediated by Rho1, Dia, and RhoGAP71E, could represent a broader paradigm in actomyosin dynamics. The capacity of the product, F-actin, to trigger negative feedback on its own synthesis via recruitment of a RhoGAP, may be used in diverse biological scenarios and be adjusted to the particular requirements of each setting. Several examples for actin negative feedback circuits were recently reported in early embryos. Bement et al. (2015) monitored the surface of starfish and frog oocytes and identified multiple successive waves of Rho activation and actin nucleation, followed by inactivation and disassembly, respectively. They speculated that these waves keep the oocyte surface undetermined, until a prominent signal for the localized recruitment of the actomyosin machinery is provided after fertilization, to generate the first cytokinetic ring. Robin et al. (2016) Preprint followed spikes of actin nucleation and disassembly during pulsed contractility of the early *C. elegans* embryo and identified two RhoGAP proteins that are recruited to the sites of actin nucleation and keep the cell surface plastic. An analogous circuitry was recently shown to regulate cell contractility in cell

culture (Graessl et al., 2017). In this case, the actin nucleation and disassembly cascade was coupled to the activity of myosin II, which may allow spontaneous patterns of subcellular contractility to explore local mechanical cues. A similar actin assembly and disassembly feedback module may contribute to other processes where dynamic waves of actin have been observed, such as in cell motility (Xiong et al., 2010; Barnhart et al., 2017) or formation of axonal protrusions (Katsuno et al., 2015).

Secretion of viscous materials from a variety of epithelial glands requires exertion of active forces, to facilitate content release from large secretory vesicles after their fusion with the apical cell membrane (Nightingale et al., 2011; Miklavc et al., 2012; Geron et al., 2013). Formation of an actin coat around each vesicle and recruitment of myosin are common features of these systems. Future work should examine whether the dynamic behavior of the actin coat and the functional significance of its disassembly, characterized here in the context of the *Drosophila* larval salivary gland, is also operating in other secretory systems.

Materials and methods

Drosophila genetics

The following *Drosophila* lines were used ("B" designates Bloomington *Drosophila* Stock Center stock number): UAS-LifeAct-Ruby (B-35545; Hatan et al., 2011), Sgs3-GFP (Biyasheva et al., 2001; B-5884), Sqh-GFP (Royou et al., 2004; B-57145), *Ubi-AniRB-D::GFP* (Rho1 sensor; Munjal et al., 2015; from T. Lecuit, Institut de Biologie du Développement, Marseille, France), UAS-*chickadee* (from L. Cooley, Yale University, New Haven, CT), UAS-*Arp3-GFP* (Hudson and Cooley, 2002; B-39721), and UAS-*chicRNAi*^{HMS00550} (B-34523). RNAi lines used for the RhoGAP screen are described in Table S1. *fkh-Gal4* was used to drive expression in salivary glands (Maybeck and Röper, 2009). For the RhoGAP screen, flies were grown at 25°C. For glands expressing RNAi

lines displayed in figures and used for further analysis, crosses were shifted to 29°C at second instar larval stage, overnight, for maximum effect of RNAi. Driver-only controls grown under the same regimen showed normal secretion.

RhoGAP71E-GFP was generated by injection of the plasmid *Splice phase 0 EGFP-FIAsH-StrepII-TEV-3xFlag* into the fly line *Mi{MIC}RhoGAP71E^{MI09170}*, as described in Venken et al. (2011).

Culturing third-instar salivary glands

After dissection in Schneider's medium, several salivary glands were placed in a chamber slide (1 μ -Slide 8-well Microscopy Chamber; Ibidi) containing 200 μ l medium. Ecdysone (5 μ M final concentration of 20-hydroxyecdysone; Sigma-Aldrich) was added to the medium immediately. For imaging, glands were transferred to a 35-mm #0 glass-bottom dish, with 14 mm Bottom Well (Cellvis D35-14-0-N), containing 200 μ l fresh medium. Glands were submerged and arranged on the bottom of the dish using forceps. The chamber slide was placed at room temperature, with light shaking for 2–3 h. Secreting glands were identified by their expanded lumen as viewed under a stereo-microscope before imaging. In many cases, salivary glands were dissected and imaged immediately, without Ecdysone addition, during their natural glue-secretion phase.

Time-lapse imaging and postimaging processing

Data were acquired with an LSM800 confocal microscope system (Zeiss), using 40 \times /1.2 (water immersion) or 20 \times /0.8 (air) objectives and 1 \times digital zoom. Typically, 18–20 z-slices were imaged at intervals of 0.5 μ m (40 \times) with a temporal resolution of 20–40 s per frame. Data acquisition for the high-time-resolution data of RhoGAP71E-GFP (Fig. S3) was performed on a single z-slice, with a temporal resolution of 4.5 s per frame. Kymographs were created using the “reslice” function in Fiji. Postimaging processing was performed using Fiji and Adobe Photoshop CS3 for cropping and adjustment of brightness/contrast, for visualization purposes only.

Drug treatment and dye injection

Each gland was imaged for at least 3 min before drug treatment to ensure overall gland health and commencement of secretion. With image acquisition stopped, ROCK inhibitor (Y-27632, 50 μ M final concentration; Sigma-Aldrich), LatA (1 μ M; Sigma-Aldrich), or jasplakinolide (2 μ M; Tocris Bioscience) were added to the medium with a micropipette, directed near but not touching the sample, and mixed slightly with a pipette tip, after which acquisition recommenced. Cultures maintained for up to 2 h after treatment did not display any overt abnormalities in tissue integrity or structure of the labeled components of the cells. For dye injection experiments, Dextran-TMR (10,000 M_w , 1 mg/ml in Schneider's medium; Molecular Probes) was injected into salivary glands during the glue-secretion phase using a Femtojet express microinjector and custom-made capillaries. Immediately after injection, glands were taken for imaging as described.

Characterization of signal dynamics

Halted vesicles were manually identified in the field of view based on the actin channel using Fiji, starting from onset of drug

addition, unless otherwise specified. For individual representative vesicles, intensity measurements were made by plotting through time the mean intensity values of a line spanning the vesicle kymograph, for each channel. Each channel was normalized to its own highest (1) and lowest (0) point to compare temporal dynamics between active Rho1 and actin. Plots were created in Excel. Characterization of pooled data from many vesicles was accomplished as described below.

Manual annotation of vesicles

A time-lapse sequence was cropped, starting from at least two time frames before actin coat appearance and continuing for the entire duration that the vesicle could be tracked. To counter movement of vesicles in the focal plane (z-position), the z-slice in which the vesicle's intensity was brightest was manually set for each time point. A vesicle's bounding box was manually drawn based on the dimensions of the vesicle with the frame of reference, manually defined as the first appearance of signal in the actin channel. Cropped time-lapse images of vesicles were rotated as needed to ensure that the bottom portion of the vesicle remained unobscured by neighboring vesicles.

Vesicle alignment

To counter vesicle movement in the x-y plane, each time frame within a vesicle's time sequence was aligned with respect to the frame of reference, using Matlab. A translation (Δx , Δy) was calculated between each frame in the sequence and the frame of reference: Morphological dilation of 3 pixels expanded the annotated bounding box to include background pixels for registration. A Gaussian filter with a width of 5 pixels and SD (σ) = 0.7 was applied to smooth both images and reduce high-frequency artifacts. The optimal translation maximized the Bhattacharyya coefficient of the normalized images with a maximal translation of 10 pixels (3.33 μ m) in each direction.

Quantifying a vesicle's dynamics

A reference line was calculated for each time frame and used to quantify a vesicle's dynamics over time. The reference line was defined as the horizontal 1-pixel-wide mask that maximizes the actin channel's median intensity within the bottom five rows from the vesicle's bounding box after being aligned according to the reference frame. All vesicles were manually examined for mistakes in reference-line vesicle identification, such as labeling of neighboring vesicles. For each channel, the mean intensity of the five brightest pixels in the reference line at each frame was recorded as the vesicle signal. The vesicle signal was smoothed in time with a Gaussian filter of window size 5 pixels and σ = 2.5. To standardize vesicle intensities and time dynamics within and across experiments, we calculated a background intensities model for each experiment. The model was designed to capture the image background pixel intensity statistics and use it for (1) correcting for photobleaching effects at the single experiment level and (2) normalizing vesicle intensities so that vesicles from different experiments could be pooled and compared. The signals of the first two time points for every vesicle were recorded as background. Background signals of all vesicles were pooled. In cases where photobleaching was identified, i.e., a significant

negative Pearson's correlation was found between background signal and time, we fitted a linear model that was used to correct the vesicle signal. Otherwise, the raw vesicle signal was used. The mean (μ) and σ of the background was used to normalize each vesicle's signal x according to the z-score measure: $x^{norm} = (x - \mu)/\sigma$, i.e., the variation from the mean background in units of SDs that can be pooled and compared across experiments.

Quantifying oscillations

Peaks were detected in the normalized vesicle signal such that peak intensity value is at least 3σ above the background and there are at least 140 s (seven frames) between two peaks. We filtered out peaks in which the dropoff values on both sides before encountering a larger value were <1.5 SD. We then scored the number of oscillations (e.g., initiations of actin cycles) in each vesicle for the Y-27632-treated glands. To correct for bias of the limited durations that vesicles could be tracked, we scored the number of oscillations only in vesicles that were tracked for at least 15.5 min, defined by the 90th percentile of times between oscillation peaks (Fig. 3 b), plus 3 s.

Quantifying signal time course

A single actin/active Rho1 cycle was calculated for each vesicle, at each channel: Vesicle background was defined as the mean z-score signal of the first two time points. The onset of the cycle was defined as the first time point at which the signal intensity exceeded 2σ above the vesicle background. Note that σ is calculated using the background from the entire gland, as described in Quantifying a vesicle's dynamics. The cycle ends once the signal falls below 2σ in relation to the vesicle's background. A vesicle is reported to be "sustained" if the signal never returns below this threshold. Cycle time for sustained vesicles is defined as the duration of the video. This characterization was used for calculation of the distribution of time course of a single actin/active Rho1 cycle (Fig. S2). For calculation of the time lag of RhoGAP71E-GFP relative to actin, we defined the onset of each signal within a vesicle as just described and subtracted time of actin signal onset from time of RhoGAP71E signal onset (Fig. S3 c).

Because of the nonuniform distribution of Rho1 on vesicles from LatA-treated glands, quantification of the duration of active Rho1 on such vesicles was performed by manual scoring of vesicles on maximum-intensity projections of images, starting 30 min after drug addition (Fig. S3 d). Vesicle contraction time under various drug treatments was also measured manually (Fig. S5 b). Bar graphs were created in Excel. BoxplotR was used to generate box plots (Spitzer et al., 2014). Nonparametric statistical tests were performed using Matlab where specified. The Matlab source code is available at <https://github.com/assafzar/DrosophilaVesicleDynamics>. It enables semiautomated quantification of molecular dynamics of contraction-arrested vesicles in the *Drosophila* salivary gland. Follow the instructions in the file DaganMain.m.

Reproducibility

At least three salivary glands (from different larvae) were examined for each genetic background and/or drug treatment, and representative images/videos are shown. Quantifications of

specific vesicle phenotypes were made on representative videos. The response to drug treatment (Y-27632, LatA, or jasplakinolide) varied between glands, although all glands showed the described phenotypes to some degree. In addition, knockdown of *RhoGAP71E* showed strong penetrance of the failed-vesicle contraction phenotype, but variable penetrance in terms of the increased duration of active Rho1 and actin cycles. In all cases, glands of varying degrees of phenotype penetrance were taken for analysis, without bias for any particular phenotype.

Online supplemental material

Fig. S1 shows that myosin II and vesicle contraction are lost upon inhibition of Rok by Y-27632. Fig. S2 provides quantitative analysis of active Rho1 and F-actin on halted vesicles, after Rok inhibition. Fig. S3 shows the effect of *RhoGAP71E* RNAi, manifested as sustained activation of Rho1 and F-actin accumulation, on inhibition of Rok. It also shows that in contraction-halted vesicles, F-actin and RhoGAP71E-GFP appear and disappear with similar dynamics. In Fig. S4, coordinated oscillations of Rho1 and F-actin are shown in contraction-halted vesicles. Fig. S5 shows that vesicle contraction is halted after *RhoGAP71E*-RNAi expression or stabilization of F-actin by jasplakinolide. Table S1 lists the nine RNAi lines targeting *RhoGAP* genes expressed in the salivary gland that were tested for their effect on actin-coat dynamics upon inhibition of Rok. Video 1 shows accumulation of contraction-halted vesicles upon inhibition of Rok. Video 2 shows that inhibition of F-actin addition by LatA does not affect the recruitment of active Rho1. Video 3 shows that knockdown of *RhoGAP71E* leads to accumulation of contraction-halted vesicles with sustained actin coats. Video 4 shows a similar result upon addition of jasplakinolide. Video 5 shows that knockdown of *chickadee* leads to failed actin-coat assembly. In Video 6, *Chickadee* was overexpressed, leading to accumulation of contraction-halted vesicles with an actin coat.

Acknowledgments

We thank Dana Meyen and Agur Wiskott for creating reagents and help with experiments. We thank L. Cooley and T. Lecuit for the UAS-*Chickadee* and active Rho1 reporter strain, respectively, and the Bloomington *Drosophila* Stock Center and Vienna *Drosophila* Resource Center for *Drosophila* lines. We are grateful to members of the B.-Z. Shilo laboratory for stimulating discussions.

This work was supported by an Israel Science Foundation grant to E.D. Schejter and B.-Z. Shilo and a National Institutes of Health grant to Gaudenz Danuser supporting A. Zaritsky (P01 GM103723). B.-Z. Shilo is an incumbent of the Hilda and Cecil Lewis chair in Molecular Genetics.

The authors declare no competing financial interests.

Author contributions: D. Segal conceived the research, developed methodologies, carried out and analyzed experiments, and wrote the manuscript. A. Zaritsky designed and carried out computational analysis of data. E.D. Schejter and B.-Z. Shilo conceived the research, supervised experiments, and wrote the manuscript.

Submitted: 2 November 2017

Revised: 24 December 2017

Accepted: 30 January 2018

References

- Barnhart, E.L., J. Allard, S.S. Lou, J.A. Theriot, and A. Mogilner. 2017. Adhesion-dependent wave generation in crawling cells. *Curr. Biol.* 27:27–38. <https://doi.org/10.1016/j.cub.2016.11.011>
- Bement, W.M., M. Leda, A.M. Moe, A.M. Kita, M.E. Larson, A.E. Golding, C. Pfeuti, K.C. Su, A.L. Miller, A.B. Goryachev, and G. von Dassow. 2015. Activator-inhibitor coupling between Rho signalling and actin assembly makes the cell cortex an excitable medium. *Nat. Cell Biol.* 17:1471–1483. <https://doi.org/10.1038/ncb3251>
- Bidlingmaier, S., and M. Snyder. 2004. Regulation of polarized growth initiation and termination cycles by the polarisome and Cdc42 regulators. *J. Cell Biol.* 164:207–218. <https://doi.org/10.1083/jcb.200307065>
- Biyasheva, A., T.V. Do, Y. Lu, M. Vaskova, and A.J. Andres. 2001. Glue secretion in the *Drosophila* salivary gland: A model for steroid-regulated exocytosis. *Dev. Biol.* 231:234–251. <https://doi.org/10.1006/dbio.2000.0126>
- Brown, J.B., N. Boley, R. Eisman, G.E. May, M.H. Stoiber, M.O. Duff, B.W. Booth, J. Wen, S. Park, A.M. Suzuki, et al. 2014. Diversity and dynamics of the *Drosophila* transcriptome. *Nature*. 512:393–399. <https://doi.org/10.1038/nature12962>
- Bubb, M.R., A.M. Senderowicz, E.A. Sausville, K.L. Duncan, and E.D. Korn. 1994. Jasplakinolide, a cytotoxic natural product, induces actin polymerization and competitively inhibits the binding of phalloidin to F-actin. *J. Biol. Chem.* 269:14869–14871.
- Burke, T.A., J.R. Christensen, E. Barone, C. Suarez, V. Sirotkin, and D.R. Kovar. 2014. Homeostatic actin cytoskeleton networks are regulated by assembly factor competition for monomers. *Curr. Biol.* 24:579–585. <https://doi.org/10.1016/j.cub.2014.01.072>
- Carvalho, A., A. Desai, and K. Oegema. 2009. Structural memory in the contractile ring makes the duration of cytokinesis independent of cell size. *Cell*. 137:926–937. <https://doi.org/10.1016/j.cell.2009.03.021>
- Cooley, L., E. Verheyen, and K. Ayers. 1992. Chickadee encodes a profilin required for intercellular cytoplasm transport during *Drosophila* oogenesis. *Cell*. 69:173–184. [https://doi.org/10.1016/0092-8674\(92\)90128-Y](https://doi.org/10.1016/0092-8674(92)90128-Y)
- Geron, E., E.D. Schejter, and B.Z. Shilo. 2013. Directing exocrine secretory vesicles to the apical membrane by actin cables generated by the formin mDial. *Proc. Natl. Acad. Sci. USA*. 110:10652–10657. <https://doi.org/10.1073/pnas.1303796110>
- Graessl, M., J. Koch, A. Calderon, D. Kamps, S. Banerjee, T. Mazel, N. Schulze, J.K. Jungkurth, R. Patwardhan, D. Solouk, et al. 2017. An excitable Rho GTPase signaling network generates dynamic subcellular contraction patterns. *J. Cell Biol.* 216:4271–4285. <https://doi.org/10.1083/jcb.201706052>
- Greenberg, L., and V. Hatini. 2011. Systematic expression and loss-of-function analysis defines spatially restricted requirements for *Drosophila* RhoGEFs and RhoGAPs in leg morphogenesis. *Mech. Dev.* 128:5–17. <https://doi.org/10.1016/j.mod.2010.09.001>
- Guillot, C., and T. Lecuit. 2013. Mechanics of epithelial tissue homeostasis and morphogenesis. *Science*. 340:1185–1189. <https://doi.org/10.1126/science.1235249>
- Hatan, M., V. Shinder, D. Israeli, F. Schnorrer, and T. Volk. 2011. The *Drosophila* blood brain barrier is maintained by GPCR-dependent dynamic actin structures. *J. Cell Biol.* 192:307–319. <https://doi.org/10.1083/jcb.201007095>
- Hudson, A.M., and L. Cooley. 2002. A subset of dynamic actin rearrangements in *Drosophila* requires the Arp2/3 complex. *J. Cell Biol.* 156:677–687. <https://doi.org/10.1083/jcb.200109065>
- Jodoin, J.N., J.S. Coravos, S. Chanet, C.G. Vasquez, M. Tworoger, E.R. Kingston, L.A. Perkins, N. Perrimon, and A.C. Martin. 2015. Stable force balance between epithelial cells arises from F-actin turnover. *Dev. Cell*. 35:685–697. <https://doi.org/10.1016/j.devcel.2015.11.018>
- Katsuno, H., M. Toriyama, Y. Hosokawa, K. Mizuno, K. Ikeda, Y. Sakumura, and N. Inagaki. 2015. Actin migration driven by directional assembly and disassembly of membrane-anchored actin filaments. *Cell Reports*. 12:648–660. <https://doi.org/10.1016/j.celrep.2015.06.048>
- Maekawa, M., T. Ishizaki, S. Boku, N. Watanabe, A. Fujita, A. Iwamatsu, T. Obinata, K. Ohashi, K. Mizuno, and S. Narumiya. 1999. Signaling from Rho to the actin cytoskeleton through protein kinases ROCK and LIM-kinase. *Science*. 285:895–898. <https://doi.org/10.1126/science.285.5429.895>
- Mason, F.M., S. Xie, C.G. Vasquez, M. Tworoger, and A.C. Martin. 2016. RhoA GTPase inhibition organizes contraction during epithelial morphogenesis. *J. Cell Biol.* 214:603–617. <https://doi.org/10.1083/jcb.201603077>
- Maybeck, V., and K. Röper. 2009. A targeted gain-of-function screen identifies genes affecting salivary gland morphogenesis/tubulogenesis in *Drosophila*. *Genetics*. 181:543–565. <https://doi.org/10.1534/genetics.108.094052>
- Miklavc, P., E. Hecht, N. Hobi, O.H. Wittekindt, P. Dietl, C. Kranz, and M. Frick. 2012. Actin coating and compression of fused secretory vesicles are essential for surfactant secretion—A role for Rho, formins and myosin II. *J. Cell Sci.* 125:2765–2774. <https://doi.org/10.1242/jcs.105262>
- Munjal, A., J.M. Philippe, E. Munro, and T. Lecuit. 2015. A self-organized biomechanical network drives shape changes during tissue morphogenesis. *Nature*. 524:351–355. <https://doi.org/10.1038/nature14603>
- Nightingale, T.D., I.J. White, E.L. Doyle, M. Turmaine, K.J. Harrison-Lavoie, K.F. Webb, L.P. Cramer, and D.F. Cutler. 2011. Actomyosin II contractility expels von Willebrand factor from Weibel–Palade bodies during exocytosis. *J. Cell Biol.* 194:613–629. <https://doi.org/10.1083/jcb.201011119>
- Pandya, P., J.L. Orgaz, and V. Sanz-Moreno. 2017. Actomyosin contractility and collective migration: May the force be with you. *Curr. Opin. Cell Biol.* 48:87–96. <https://doi.org/10.1016/j.cceb.2017.06.006>
- Robin, F.B., J.B. Michaux, W.M. McFadden, and E.M. Munro. 2016. Excitable RhoA dynamics drive pulsed contractions in the early *C. elegans* embryo. *bioRxiv*. doi: 10.1101/076356 (Preprint posted September 21, 2016)
- Rotty, J.D., C. Wu, E.M. Haynes, C. Suarez, J.D. Winkelman, H.E. Johnson, J.M. Haugh, D.R. Kovar, and J.E. Bear. 2015. Profilin-1 serves as a gatekeeper for actin assembly by Arp2/3-dependent and -independent pathways. *Dev. Cell*. 32:54–67. <https://doi.org/10.1016/j.devcel.2014.10.026>
- Rouso, T., A.M. Shewan, K.E. Mostov, E.D. Schejter, and B.Z. Shilo. 2013. Apical targeting of the formin Diaphanous in *Drosophila* tubular epithelia. *eLife*. 2:e00666. <https://doi.org/10.7554/eLife.00666>
- Rouso, T., E.D. Schejter, and B.Z. Shilo. 2016. Orchestrated content release from *Drosophila* glue-protein vesicles by a contractile actomyosin network. *Nat. Cell Biol.* 18:181–190. <https://doi.org/10.1038/ncb3288>
- Royou, A., C. Field, J.C. Sisson, W. Sullivan, and R. Karess. 2004. Reassessing the role and dynamics of nonmuscle myosin II during furrow formation in early *Drosophila* embryos. *Mol. Biol. Cell*. 15:838–850. <https://doi.org/10.1091/mbc.E03-06-0440>
- Rubinstein, B.Y., and A. Mogilner. 2017. Myosin clusters of finite size develop contractile stress in 1D random actin arrays. *Biophys. J.* 113:937–947. <https://doi.org/10.1016/j.bpj.2017.07.003>
- Shields, A.R., A.C. Spence, Y.M. Yamashita, E.L. Davies, and M.T. Fuller. 2014. The actin-binding protein profilin is required for germline stem cell maintenance and germ cell enclosure by somatic cyst cells. *Development*. 141:73–82. <https://doi.org/10.1242/dev.101931>
- Slaughter, B.D., S.E. Smith, and R. Li. 2009. Symmetry breaking in the life cycle of the budding yeast. *Cold Spring Harb. Perspect. Biol.* 1:a003384. <https://doi.org/10.1101/cshperspect.a003384>
- Spitzer, M., J. Wildenhain, J. Rappsilber, and M. Tyers. 2014. BoxPlotR: A web tool for generation of box plots. *Nat. Methods*. 11:121–122. <https://doi.org/10.1038/nmeth.2811>
- Suarez, C., R.T. Carroll, T.A. Burke, J.R. Christensen, A.J. Bestul, J.A. Sees, M.L. James, V. Sirotkin, and D.R. Kovar. 2015. Profilin regulates F-actin network homeostasis by favoring formin over Arp2/3 complex. *Dev. Cell*. 32:43–53. <https://doi.org/10.1016/j.devcel.2014.10.027>
- Tcherkezian, J., and N. Lamarche-Vane. 2007. Current knowledge of the large RhoGAP family of proteins. *Biol. Cell*. 99:67–86. <https://doi.org/10.1042/BC20060086>
- Tran, D.T., and K.G. Ten Hagen. 2017. Real-time insights into regulated exocytosis. *J. Cell Sci.* 130:1355–1363. <https://doi.org/10.1242/jcs.193425>
- Tran, D.T., A. Masedunskas, R. Weigert, and K.G. Ten Hagen. 2015. Arp2/3-mediated F-actin formation controls regulated exocytosis in vivo. *Nat. Commun.* 6:10098. <https://doi.org/10.1038/ncomms10098>
- Uehata, M., T. Ishizaki, H. Satoh, T. Ono, T. Kawahara, T. Morishita, H. Tamakawa, K. Yamagami, J. Inui, M. Maekawa, and S. Narumiya. 1997. Calcium sensitization of smooth muscle mediated by a Rho-associated protein kinase in hypertension. *Nature*. 389:990–994. <https://doi.org/10.1038/40187>
- Vavylonis, D., J.Q. Wu, S. Hao, B. O'Shaughnessy, and T.D. Pollard. 2008. Assembly mechanism of the contractile ring for cytokinesis by fission yeast. *Science*. 319:97–100. <https://doi.org/10.1126/science.1151086>
- Venken, K.J., K.L. Schulze, N.A. Haelterman, H. Pan, Y. He, M. Evans-Holm, J.W. Carlson, R.W. Levis, A.C. Spradling, R.A. Hoskins, and H.J. Bellen. 2011. MiMIC: A highly versatile transposon insertion resource for engineering *Drosophila melanogaster* genes. *Nat. Methods*. 8:737–743. <https://doi.org/10.1038/nmeth.1662>
- Xiong, Y., C.H. Huang, P.A. Iglesias, and P.N. Devreotes. 2010. Cells navigate with a local-excitation, global-inhibition-biased excitable network. *Proc. Natl. Acad. Sci. USA*. 107:17079–17086. <https://doi.org/10.1073/pnas.1011271107>